Clay Minerals, (2010) **45**, 209–224

A hydrothermal clay mineral assemblage at the Late Proterozoic unconformity in the Buenos Aires Complex – La Tinta Formation, Barker area, Tandilia Ranges (Argentina)

Presented at the XIV International Clay Conference, Castellaneta Marina, Italy, June 2009

J. C. MARTÍNEZ[1,*], J. A. DRISTAS[2], H.-J. MASSONNE[3] AND T. THEYE[3]

[1] *CONICET-INGEOSUR and Departamento de Geología, San Juan 670, UNS, Bahía Blanca, 8000, Argentina,*
[2] *CIC, INGEOSUR and Departamento de Geología, San Juan 670, UNS, Bahía Blanca, 8000, Argentina, and*
[3] *Institut für Mineralogie und Kristallchemie, Universität Stuttgart, Azenbergstrasse 18, D-70174, Germany*

(*Received 11 September 2009; revised 30 December 2009; Editor: John Adams*)

ABSTRACT: A general alteration pattern of two transitional clay mineral assemblages was determined by petrography and X-ray diffractometry studies at the Tandilia Late Proterozoic unconformity zone, around the Barker locality: (1) K-white mica + chlorite + calcite ± anatase-rutile ± secondary quartz (farther from the unconformity) and (2) pyrophyllite + K-white mica + Ti-rich hematite ± aluminium phosphate-sulphate minerals ± tourmaline ± anatase-rutile (closer to the unconformity). The local occurrence of Na in K-white micas and K-Na in pyrophyllite is described for the first time. Possible interlayering with intermediate K-Na mica and paragonite is indicated by detailed X-ray diffraction analyses. A negative Eu anomaly (Eu/Eu* = 0.24), strongly positive Eu anomaly (Eu/Eu* =11.7) and positive Ce anomaly characterized rapid changes from an unaltered basement to the most altered basement and sedimentary rocks at the unconformity. Aluminium phosphate-sulphate minerals dominate patterns of *LREE*. A model of hydrothermal alteration comparable to that of unconformity-related uranium deposits is presented.

KEYWORDS: Late-Proterozoic unconformity, clay mineral assemblage, hydrothermal alteration, Barker area, Argentina.

The igneous-metamorphic basement of the Buenos Aires Complex (Di Paola & Marchese, 1975) in eastern Argentina is composed of granitoids, migmatites, amphibolites, gneisses including mylonites, metavolcanic rocks and marbles (e.g. Cingolani & Dalla Salda, 2000; Pankhurst *et al.*, 2003; Delpino & Dristas, 2008). A wide range of ages for this basement, the southernmost part of the Río de la Plata Craton, is mainly related to the Transamazonian orogeny, ~2200–1800 Ma (Cingolani & Dalla Salda, 2000). A Neoproterozoic–Early Palaeozoic shallow marine succession, the La Tinta Fm. (Leveratto & Marchese, 1983), unconformably overlies the large crystalline lithological variety of basement rocks. A very low-grade metamorphism (anchizonal) has been proposed to explain the secondary mineral assemblages and a general spreading out of Rb-Sr ages for this sedimentary succession (Bonhomme &

* E-mail: jcmartin@uns.edu.ar
DOI: 10.1180/claymin.2010.045.2.209

Cingolani, 1980; Zalba *et al.*, 1982). Besides, hydrothermal breccias and associated clay deposits have been recognized, affecting the middle-upper part of the sedimentary cover (Dristas & Frisicale, 1992; Frisicale, 1991). An age of 787±22 Ma (K/Ar) was obtained for the lower section of the La Tinta Fm. (Dristas & Martínez, 2007).

The alteration recognized in the unconformity zone between the Buenos Aires Complex (BAC) and the La Tinta Fm. (LTF) in the Tandilia Ranges has been under discussion since processes of weathering, hydrothermal metasomatism and even metamorphism were assigned to explain the mineral parageneses in this zone (Dristas & Frisicale, 1984; Frisicale, 1991; Andreis *et al.*, 1992; Zalba *et al.*, 1992; Frisicale & Dristas, 1993; Zalba & Andreis, 1998; Dristas *et al.*, 2003; Dristas & Martínez, 2007; Martínez & Dristas, 2007). In the unconformity zone exposed in the western San Manuel Hills, approximately 50 km SE of the village of Barker, mineral assemblages containing pyrophyllite, kaolinite, sericite, diaspore, tourmaline, rutile, alunite, hematite-goethite, secondary quartz, calcite and baryte were initially ascribed to hydrothermal alteration zoning (Dristas & Frisicale, 1984). The formation of these minerals was explained by argillic alteration at relatively high temperatures, affecting the rocks on both sides of the unconformity. Later, this alteration was reinterpreted as a result of complex processes combining weathering, hydrothermal interaction and metamorphism (Zalba *et al.*, 1992). In the Barker area, not only rare alteration profiles have been studied at the unconformity, but also geographically scattered profiles have been described by Dristas & Martínez (2007) and Martínez & Dristas (2007). In these works, two alteration fronts were generally established according to the mineral alteration parageneses asymmetrically distributed with respect to their pervasiveness in basement and sedimentary rocks.

In this paper we describe many alteration profiles, spread over a wide area, determined by petrography and X-ray diffraction (XRD). We establish a direct relationship between *REE* patterns of rocks progressively more altered in the unconformity zone with secondary mineral assemblages. This is combined with systematic electron microprobe analysis (EMPA) of K-white micas and pyrophyllites, the most abundant minerals present as phyllic alteration in the unconformity zone which have not been chemically characterized until now. Petrographic observations on affected rocks reveal typical alteration and replacement textures common to both sides of the unconformity. The alteration model in which hot fluid circulation was controlled by an unconformity is comparable to unconformity-related U deposits from the East Alligator Rivers Uranium Field, Northern Australia, and the Athabasca Basin, Canada (Komninou & Sverjensky, 1995; Lorilleux *et al.*, 2003; Beaufort *et al.*, 2005; Gaboreau *et al.*, 2005).

GEOLOGICAL SETTING

The area studied, neighbouring the locality of Barker, covers an area >350 km^2. Igneous-metamorphic rocks of the Buenos Aires Complex (BAC) discontinuously crop out at the northern side of NE trending ranges formed by the overlying sedimentary succession. In the Cuchilla de Las Aguilas range, NE of Barker (Fig. 1), the BAC is composed of medium- to coarse-grained granodioritic to tonalitic migmatites with amphibolite lenses <1.5 m wide. Its regional foliation of subvertical aptitude ranges from N70ºW to N60ºW. Apparently non-deformed granodioritic to tonalitic granitoids crop out north of the La Siempre Verde ranch (Fig. 1) in the north-central portion of the Barker-Villa Cacique sector. On the other hand, tectonically banded (N90ºE) light-grey migmatites dominate the basement of the north-easterly outcrops.

The BAC is covered by a sedimentary platform succession, the La Tinta Formation (LTF), which dips slightly (3–6º) to the SW (Leveratto & Marchese, 1983). Normal faults with a few metres of displacement, subvertical position and basement-inherited strike (N90ºE and NW–SE) define a block structure for the sedimentary succession. The unconformity surface studied near Barker, one of the ancient unconformities of southern South America, is named here the Tandilia Late-Proterozoic Unconformity (TLPU).

Siliciclastic sedimentary rocks of the LTF, mainly quartz arenites, build up the characteristic plateau-like hills and ranges. Marls and limestones from the continuous sedimentary succession dominate the southern side, representing the upper part of the sedimentary succession in the Villa Cacique sector (Fig. 1). Clay mining is carried out widely at several levels of the lower and medium siliciclastic succession and an open pit quarry is situated in the southern sector over the limestones (Loma Negra

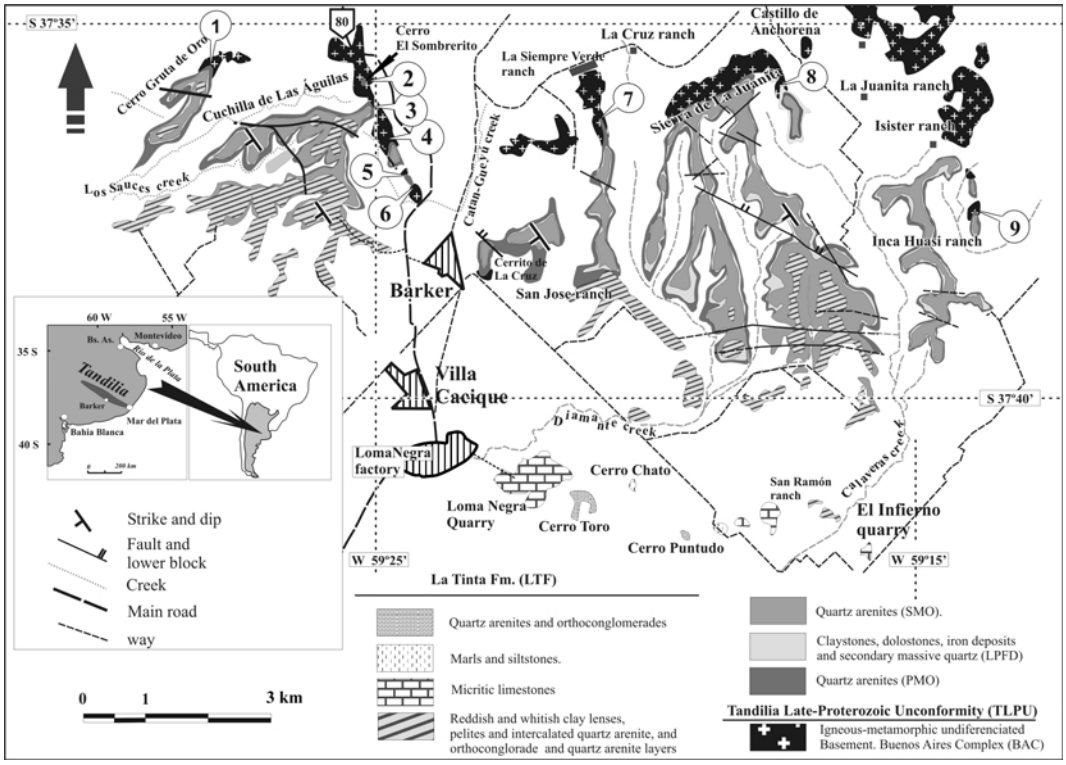

FIG. 1. Geological sketch map of the profiles studied adapted from Leveratto & Marchese (1983) and Manassero (1986). (1) East of Cerro Gruta de Oro hill; (2) Cerro El Sombrerito hill; (3) East of Cuchilla de Las Aguilas range; (4) North of Cerro del Medio hill; (5) North of Cerro Chico hill; (6) South of Cerro Chico hill; (7) North of La Siempre Verde ranch; (8) north of La Juanita range, and (9) north of a small hill to the east of the Inca Huasi ranch.

Quarry). The complete sedimentary succession is found here over <200 m and thinner than in the Olavarría area, located 100 km to the NW.

ANALYTICAL METHODS

Transmitted light petrographic observations were crucial for identification of replacement and *in situ* crystallization textures. Clay mineral identification was carried out with a Rigaku-Denki Geiger Flex Max III C X-ray diffractometer at the Departamento de Geología (UNS), Bahía Blanca (Argentina). Agate mill-powdered samples were scanned using Cu-$K\alpha$ radiation (λ = 1.54 nm) under 35 kV, 15 mA conditions, where step-scan data were collected from 3 to 65º2θ using a step size of 0.04º2θ s^{-1} for routine procedure and 0.01º2θ s^{-1} for more accurate determinations of discrete quantities of paragonite and intermediate K-Na white mica, recorded from 3 to 30º2θ. The spectrometer data were handled with MDI DataScan 4 software. Bulk-rock chemical analyses of 30 samples of altered rocks at the unconformity and fresh basement were carried out by ACTLABS (Activation laboratories Ltd., Ontario, Canada). For such analyses, X-ray fluorescence for major elements, and inductively coupled plasma mass spectrometry for trace elements and rare earth elements (*REE*) were applied.

On the basis of previous petrography, XRD and bulk-rock chemistry determinations, 13 representative samples were selected for systematic EMP analysis. Wavelength-dispersive spectrometry (WDS) was performed at the Institut für Mineralogie und Kristallchemie, Universität Stuttgart, Germany, with a Cameca SX100 equipped with five spectrometers (analytical crys-

tals: LLIF, TAP (2), PET, LPET). 'Virtual WDS' (Reed & Buckley, 1998), software was used to check for spectral interferences. Natural and synthetic standards were: K-feldspar (Si, Al, K), rhodonite (Mn), Fe_2O_3 (Fe), baryte (Ba) $LaPO_4$ (La), rutile (Ti), albite (Na), Cr_3O_2 (Cr), diopside (Ca, Si, Mg), calcite (Ca), fluorite (F), $EuPO_4$ (Eu), $CePO_4$ (Ce), NaCl (Cl), Th-glass (Th), celestine (Sr), apatite (P, Ca) and U-glass (U). Suitable operating conditions were selected for each analysed mineral in order to avoid beam damage. A voltage of 15 kV was combined with a beam current ranging from 7 to 10 nA, a take off angle of 40º, and a variable spot beam diameter (2–15 μm). Manual, point by point, measurements were carried out due to the small crystal sizes that frequently require spatial accuracy. Structural formulae were calculated based on 22 positive charges for K-white micas and pyrophyllites.

RESULTS

Petrography of unaltered basement

The basement cropping out in the northwest (Fig. 1, profiles 1–6) is represented by heterogeneously deformed granodioritic to tonalitic migmatites with a preferential N70ºW to N60ºW strike and subvertical dip. Leucosome consists of plagioclase (mainly $Ab_{60}An_{40}$), quartz, scarce orthoclase-microcline and rare garnet. Melanosome is biotite-rich. Metamorphic retrograde minerals are sericite and epidote after feldspars, and chlorite and epidote after biotite and garnet. Accessory minerals include apatite, zircon, allanite and monazite. Medium to fine-grained granoblastic to nematoblastic amphibolite lenses are spatially layered in migmatites. Its metamorphic mineral assemblage is hornblende, plagioclase and minor quartz.

To the NE (Fig. 1, profiles 8–9), banded xenoblastic migmatites have granitic to granodioritic compositions. Perthitic microcline is rather more abundant than andesine, biotite is pseudomorphically replaced by muscovite, and quartz is mostly found in myrmekites. Metamorphic retrograde and accessory minerals are the same as those found in the NW outcrops.

To the north of the La Siempre Verde ranch (Fig. 1, profile 7), a hypidiomorphic equigranular granitoid crops out 9 m below the unconformity. It is composed of plagioclase (andesine, 45%), quartz (30%), biotite (12%) and K-feldspar (8%).

Petrography of the altered basement

The basement is increasingly altered to the TLPU. Generally, 20–8 m below the TLPU, calcite, chlorite and fine-grained sericite are present as veins and patches in pervasively altered basement rocks. The calcite and chlorite become scarce close to the TLPU, where an intense phyllic alteration predominates. Aggregates of secondary chlorite were classified as ripidolite $[(Mg,Fe^{2+})_9Al_6Si_5O_{20}(OH)_{16}]$ (Dristas & Martínez, 2007).

Immediately below the TLPU, the original basement rocks, strongly metasomatized, have lost their igneous-metamorphic structure to show a horizontal and irregular pseudo-foliation. There, scarce and isolated granoblastic quartz grains are immersed in the phyllic alteration matrix, mainly composed of sericite and/or pyrophyllite. Curved flakes of pyrophyllite and/or sericite fill marked corrosion embayments in quartz grains to show a swirl-like texture (Fig. 2a). This replacement texture is also common to quartz grains of altered sandstone of the LTF at the TLPU.

To the north of the La Juanita Range (Fig. 1, profile 8), the basement shows completely chloritized and sericitized biotite flakes containing Fe oxides far from the TLPU. This alteration profile is characterized by complete replacement by microcrystalline quartz (Fig. 2b), commonly disrupted by microfractures 2 m below the unconformity. Kaolinite crystal flakes (<250 μm), goethite-dyed, and sericite are intergranular.

Aluminium phosphate-sulphate (APS) minerals are scattered or clustered in the alteration matrix (Fig. 3b,c) composed of sericite and/or pyrophyllite. As a rule they appear close to the TLPU, where intense metasomatism of original protoliths had occurred. These crystals are recognizable as <6 μm in size, high relief, slightly yellow colour and low birefringence in transmitted light. Tourmaline is another rare secondary mineral immersed in a phyllic alteration product, forming prismatic crystals up to 500 μm in length.

Hematite and goethite after biotite and opaque minerals, dying the altered rocks, are ubiquitous through different profiles, partially forming small veins. Nests of platy Ti-rich hematite were identified in the Cerro del Medio basement and at the base of corroded bimodal quartz arenites. This hematite contains inclusions of siderite and baryte identified by EDS (Dristas & Martínez, 2007). Rutile and anatase crystals are also ubiquitous, but

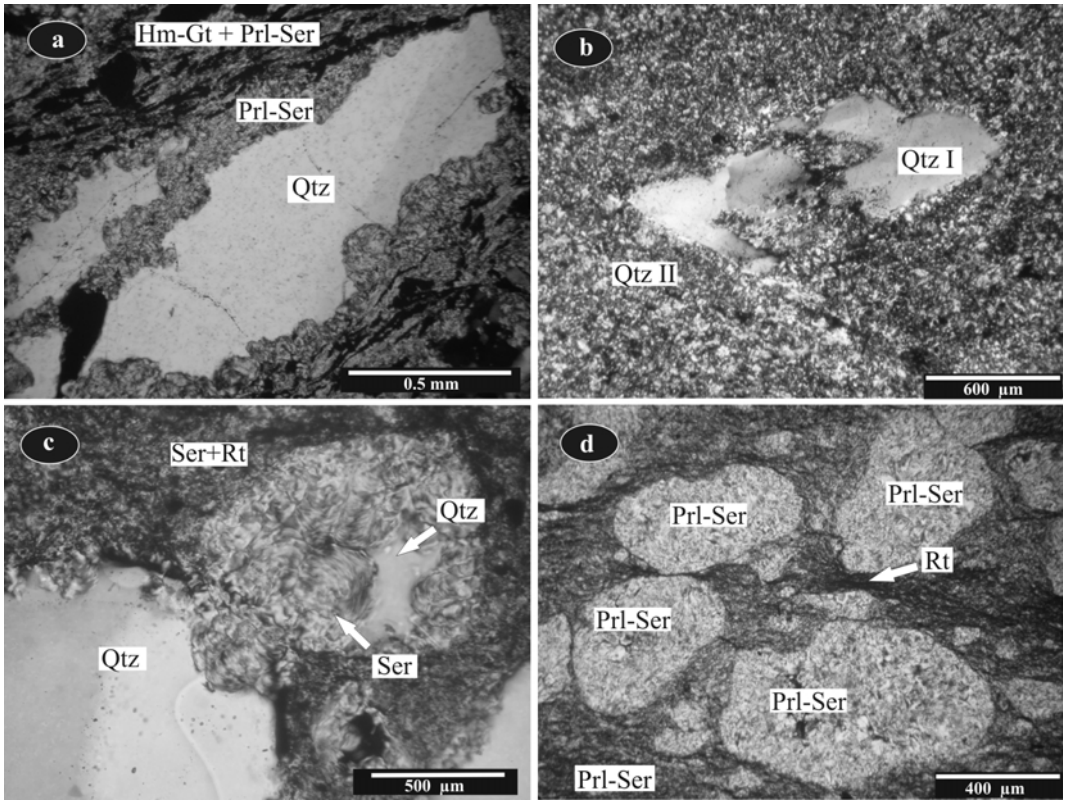

FIG. 2. Photomicrographs using transmitted light. Mineralogy established by petrography and XRD. (a) Metamorphic quartz crystal partly corroded and replaced by the swirl-like texture of a clay matrix of pyrophyllite and sericite (Prl-Ser), which is penetrated by hematite-goethite (Hm-Gt). Basement from the north of La Siempre Verde ranch (crossed polars). (b) Relict of metamorphic quartz (Qtz I) of basement replaced by microcrystalline quartz (Qtz II) from north of the Sierra de la Juanita range (crossed polars). (c) Pseudomorphic replacement of rounded quartz clasts from a quartz arenite-wacke at the TLPU by pyrophyllite and sericite into an alteration matrix of Prl + Ser + rutile (Rt). North of the La Siempre Verde ranch (crossed polars). (d) Quartz (Qtz) clasts from a sandstone wacke at the TLPU replaced, totally to partly, by sericite (Ser). The alteration matrix is formed by Ser + Rt. North of Sierra de la Juanita (crossed polars).

more abundant where metamorphic micas, biotite and muscovite, are completely obliterated.

Petrography of altered sandstones

Sandstones from the base of the LTF include homometric to bimodal quartz arenites, occasionally coarse grained. In some profiles, quartz grains are immersed in a matrix of sericite and/or pyrophyllite and with signs of incipient to intense corrosion with swirl-like texture development (Fig. 2c–d). In such cases, the original protolith is not easy to recognize either as quartz arenites or wackes.

In heavily cemented quartz arenites the syntaxial diagenetic overgrowth could be corroded. Chlorite, daphnite (Dristas & Martínez, 2007) and platy Ti-rich hematite frequently crystallized in corrosion voids. A subsequent veining of hematite-goethite and secondary quartz crosscut these rocks.

Chemical composition of K-white micas and pyrophyllites

Chemical analyses by EMPA of phyllosilicates in 13 samples of the altered BAC and LTF at the unconformity allowed us to identify and charac-

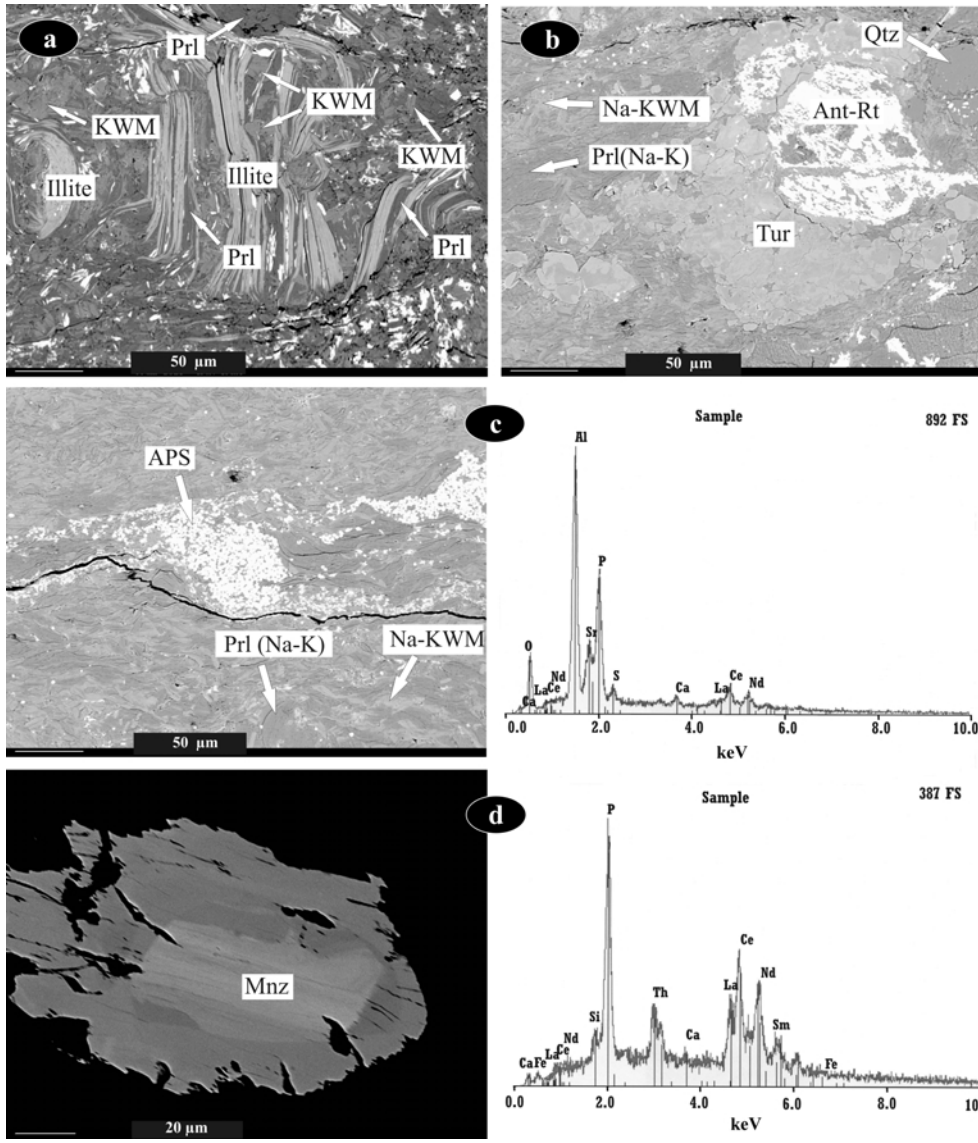

FIG. 3. Backscattered electron images of samples from the TLPU zone, Barker area. (a) Illitized metamorphic K-white mica (Illite) in an alteration matrix of pyrophyllite (Prl) and secondary K-white mica (KWM). Basement north of La Siempre Verde Ranch. (b,c) Basement completely altered to Na-K bearing pyrophyllite (Prl (Na-K)), K-white mica with Na (Na-KWM), tourmaline crystals (Tur), APS minerals and anatase-rutile (Anat-Rt) (northeast of Inca Huasi ranch). In (c) the EDS spectrum of APS minerals is shown on the right. (d) Zoned monazite (Mnz) crystal in biotite of the fresh migmatite from north of the Sierra de La Juanita range and EDS spectrum of monazite crystal.

terize minerals such as K-white micas with paragonite content and pyrophyllite as the main minerals of the phyllic alteration. For the calculation of structural formulae from EMPA, 22 positive charges were used. Our K-white micas have values of Σoxide >90%, Si >3.00, Σ(Na+Ca+K) >0.8 and a Ca content <0.05 a.p.f.u. According to the IMA subcommittee report (Rieder *et al.*, 1998), most of

our K-white micas are true micas (having >50% of monovalent cations as interlayer cations and exhibiting 2.0−0.85 interlayer cations) and dioctahedral (containing <2.5 octahedral cations per formula unit). Only altered potassic mica analyses point to interlayer-deficient micas as their interlayer cation content is <0.85 (illite).

EMPA of four groups of K-white micas were plotted in correlation diagrams (in a.p.f.u) of Si *vs.* Na/(Na+K+Ca) and Mg + $Fe_{(tot)}$ + Si *vs.* ^{IV}Al + ^{VI}Al (Fig. 4a,b). The chemical compositions of representative potassic white micas are given in Table 1. All Fe obtained by EMPA was arbitrarily assumed to be Fe^{2+} for micas from the unaltered basement. On the other hand, all Fe in secondary potassic white micas of the altered basement and sandstones at the TLPU and in altered micas (relict) in basement is arbitrarily recalculated as Fe^{3+}, since these micas are associated with Fe oxides.

The first group corresponds to potassic white micas (KWM) of the fresh xenoblastic migmatites of the BAC. These micas are characterized by a slight variation in their interlayer cation occupancy with a relatively ideal K ($\approx$ 1 a.p.f.u) and small Na (<0.05 a.p.f.u) content for muscovites. Si contents are 3.15−3.03 a.p.f.u.

Secondary mica of the altered basement (Fig. 3b,c) and the matrix of sandstones at the

TABLE 1. Representative EMP analyses of K-white mica (KWM) and pyrophyllite (Prl) given as wt.% oxide and recalculated as structural formulae. Localities: (1, 2, 4, 6, 9, 11) NE of Inca Huasi ranch, (3, 5) N of the Sierra de la Juanita, (7, 8, 10, 12) N of La Siempre Verde ranch.

	KWM of fresh basement		Secondary KWM of altered rocks				Illitized KWM of altered basement		Prl of altered rocks			
			Basement		Sed. rocks				Basement		Sed. rocks	
	1	2	3	4	5	6	7	8	9	10	11	12
SiO_2	47.87	47.65	47.96	47.86	46.40	46.62	43.64	44.67	51.10	65.18	60.48	65.21
TiO_2	0.91	1.57	0.03	0.01	0.02	0.04	2.87	2.91	0.02	0.06	0.03	0.01
Al_2O_3	34.18	33.96	36.01	37.72	37.26	37.76	25.16	24.71	38.65	28.94	33.88	28.57
FeO	1.78	1.89							0.45	0.29	0.37	0.43
Fe_2O_3			2.26	1.14	1.33	1.31	11.69	11.51				
MnO	0.05	0.02	0.00	0.01	0.00	0.00	0.01	0.00	0.00	0.00	0.00	0.00
MgO	1.24	1.28	0.30	0.03	0.12	0.09	0.85	0.54	0.09	0.02	0.06	0.00
CaO	0.00	0.00	0.13	0.01	0.04	0.01	0.05	0.08	0.13	0.01	0.17	0.00
Na_2O	0.36	0.32	0.24	1.24	1.58	0.95	0.21	0.22	3.73	0.23	1.70	0.06
BaO	0.58	0.87	0.01	0.09	0.09	0.11	0.42	0.49	0.02	0.00	0.00	0.00
K_2O	11.01	10.81	9.98	8.38	7.98	9.23	8.76	8.30	3.31	0.27	1.02	0.15
Total	97.97	98.36	96.92	96.49	94.82	96.12	93.66	93.43	97.49	95.00	97.69	94.43
Number of ions based on 22 positive charges – Fe* is either Fe^{2+} or Fe^{3+}												
Si	3.125	3.106	3.115	3.090	3.055	3.043	3.067	3.130	3.177	3.933	3.60	3.953
$Al^{(IV)}$	0.875	0.894	0.885	0.910	0.945	0.957	0.933	0.870	0.823	0.067	0.380	0.047
Ti	0.045	0.077	0.001	0.000	0.001	0.000	0.152	0.153	0.001	0.003	0.001	0.000
$Al^{(VI)}$	1.755	1.716	1.872	1.961	1.946	1.948	1.151	1.171	2.009	1.991	2.010	1.994
Fe*	0.097	0.103	0.111	0.055	0.066	0.064	0.618	0.607	0.023	0.015	0.019	0.022
Mn	0.003	0.001	0.000	0.000	0.000	0.000	0.001	0.000	0.000	0.000	0.000	0.000
Mg	0.121	0.124	0.029	0.003	0.012	0.008	0.089	0.056	0.008	0.002	0.005	0.000
ΣOct	2.020	2.021	2.012	2.021	2.025	2.022	2.009	1.987	2.041	2.011	2.035	2.017
Ca	0.000	0.000	0.009	0.001	0.003	0.001	0.003	0.006	0.009	0.001	0.011	0.000
Na	0.045	0.040	0.030	0.155	0.201	0.120	0.028	0.030	0.450	0.027	0.197	0.007
K	0.917	0.899	0.827	0.690	0.669	0.769	0.785	0.742	0.263	0.021	0.078	0.012
Ba	0.059	0.088	0.001	0.009	0.009	0.011	0.046	0.054	0.002	0.000	0.000	0.000
ΣCations	1.021	1.028	0.867	0.854	0.883	0.901	0.863	0.832	0.723	0.048	0.286	0.019
Na* = Na/(Na+K+Ca)	0.047	0.043	0.034	0.183	0.231	0.135	0.035	0.038				

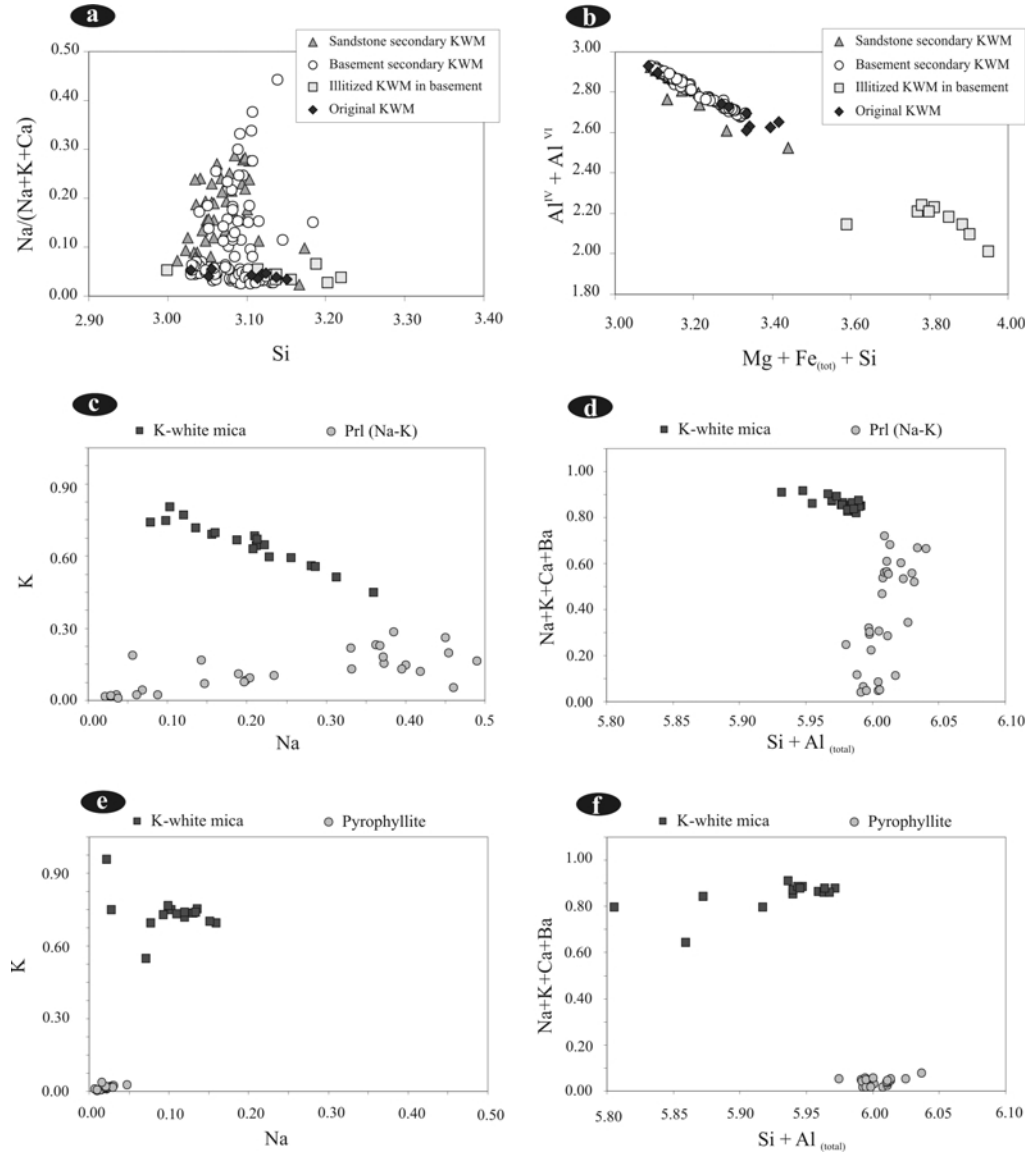

FIG. 4. (a–b) Correlation plots of EMPA data (in a.p.f.u) for analysed potassic white mica at the TLPU: (a) Si *vs.* Na/(Na+K+Ca) (paragonitic substitution for interlayer cation). (b) Mg + $Fe_{(tot)}$ + Si *vs.* ^{VI}Al + ^{IV}Al showing Tschermak substitution in four groups of K-white micas (where $Fe_{(tot)}$ is Fe^{2+} and Fe^{3+}). (c–e) Correlation plots of EMPA data (in a.p.f.u) for K-white mica and pyrophyllite of altered basement and sedimentary rocks at the TLPU zone: K *vs.* Na and Na+K+Ca+Ba *vs.* Si + $Al_{(total)}$. (c,d) Profile northeast of Inca Huasi ranch. (e,f) Profile north of the La Siempre Verde ranch.

TLPU (Fig. 2c–d) forming groups **2** and **3** of Fig. 4 are chemically identical. A group of these micas displays clear paragonite contents [Na* = Na/(Na+K+Ca)] (Fig. 4a) with a maximum of Na* = 0.45. Interlayer cations K-Na have a negative correlation (correlation factor = 0.96). Other characteristics of the K-white micas of groups **2** and **3** are their relatively large Si contents

between 3.01 and 3.17 a.p.f.u and an occupancy of octahedral cations (Al, Fe, Mg and Mn) around 2.02–2.03 a.p.f.u.

Group 4 (Fig. 4) corresponds to illitized potassic white mica with large Fe^{3+} (0.51–0.62 a.p.f.u), Ti (0.15–0.38 a.p.f.u) and Ba (0.04–0.06 a.p.f.u) contents. A relatively small ^{VI}Al occupancy also characterizes these illitized K-white micas. Flake textural relationships with secondary phyllosilicates (Fig. 3a) point to an altered white mica which can be recognized in backscattered electron images.

Large values of Fe contents could be introduced into white micas by the Tschermak's substitution [$(Mg,Fe^{2+}) + Si = {}^{VI}Al + {}^{IV}Al$)], the ferrimuscovite substitution ($Fe^{3+} = {}^{VI}Al$) and a substitution of Ti coupled with Fe ($Fe^{2+} + Ti^{4+} = 2\ {}^{VI}Al$) and possibly also by the substitution $Fe^{3+} = {}^{IV}Al$ (Fleet, 2003). Unfortunately, the latter substitution and the ferrimuscovite substitution require the determination of Fe^{3+}. Although this is not possible with EMPA, the coexistence with hematite (large f_{O_2}), the good correlation between Σ(Fe+Mg+Mn) value and ^{VI}Al, and the apparent large octahedral occupancy when the mica structural formula is calculated with Fe^{2+} only (Massonne, 1995) suggest the existence of Fe^{3+} in the white-mica and thus of a ferrimuscovite component.

Pyrophyllite was recognized in altered rocks from several profiles through the unconformity by XRD, but only backscattered electron images offered clear textural relationship. Representative data of analysed pyrophyllites are shown in Table 1 (analyses 9–12). Feldspars (microcline, plagioclase and orthoclase) are completely replaced by K-white mica and/or pyrophyllite and no traces of them remain where the rocks were strongly altered.

A comparison between K-white micas and pyrophyllites, found on both sides of the TLPU in the alteration profiles NE of Inca Huasi ranch and north of the La Siempre Verde ranch, is shown in Fig. 4c–f. At the former locality, K-white micas with paragonite content and pyrophyllites with apparent variable contents of Na-K (Fig. 4c) form the clay mineral assemblage immediately below and above the TLPU. A negative Na-K correlation in pyrophyllite chemistry has been obtained. Texturally, these micas are present in the basement and sandstone as an alteration matrix (Fig. 3b,c), frequently dyed by goethite-hematite, and as swirl-like textures in corrosion embayments of quartz (Fig. 2b,d). Values of Na+K+Ca+Ba are <0.7 a.p.f.u. and very variable for the pyrophyllite EMP analyses (Fig. 4d). The maximum Na and K content in analysed pyrophyllite are almost 1.0 a.p.f.u. and 0.6 a.p.f.u., respectively.

The Na contents of dioctahedral K-white micas and the Na-K contents in pyrophyllite could be linked either to solid solution or to phases finely intergrown for each main mineral species, since this could not be detected on the EMPA resolution scale (Shau *et al*., 1991).

In the western profile, north of the La Siempre Verde ranch, the mineral assemblage Prl + KWM ± Kln is common in both intensely altered rocks of the basement and the sedimentary cover. Plots of Na (a.p.f.u) *vs.* K (a.p.f.u) and $Si+Al_{(total)}$ *vs.* Na+K+Ca (Fig. 4e,f) indicate that neither K-white mica with paragonite content nor pyrophyllite with Na-K content exist in these clay mineral alterations. There, pyrophyllite is situated in corrosion embayments of epiclastic quartz from sandstones and quartz crystals of basement rocks. Potassic white mica (fine-grained flakes) and pyrophyllite occur in the alteration matrix together with APS minerals in both altered rock types.

In the alteration profile north of Sierra de la Juanita, pyrophyllite is absent, but kaolinite is present about 2 m away from the TLPU where the basement is massively silicified by microcrystalline quartz. The secondary potassic white mica of the altered basement shows a more limited K-Na variation than the mica of the alteration matrix of the sandstone above the TLPU.

X-ray powder diffraction data

XRD patterns of samples with K-white micas with Na contents and pyrophyllite with K-Na contents determined with EMPA were studied carefully. Two major 002 reflection peaks (Fig. 5a) of values of 9.984 and 9.226 Å correspond to muscovite (Ms) $2M_1$-1M and pyrophyllite (Prl), respectively. In the zone of 004 basal reflection (Fig. 5b) corresponding *d* values are 5.00, 4.961 and 4.609 Å for muscovite 1M, muscovite $2M_1$ and pyrophyllite, respectively. The higher-order basal reflections were better defined (Fig. 5c) with 3.332 Å and 3.191 Å for muscovite and 3.069 Å for pyrophyllite. Discrete quantities of additional micaceous phases could be assigned to intermediate K-Na white micas (Im) and paragonite (Pg) as discrete series of basal reflections were recognized. In Fig. 5a reflection peaks 9.784 Å and 9.656 Å correspond to Im and Pg, respectively. The

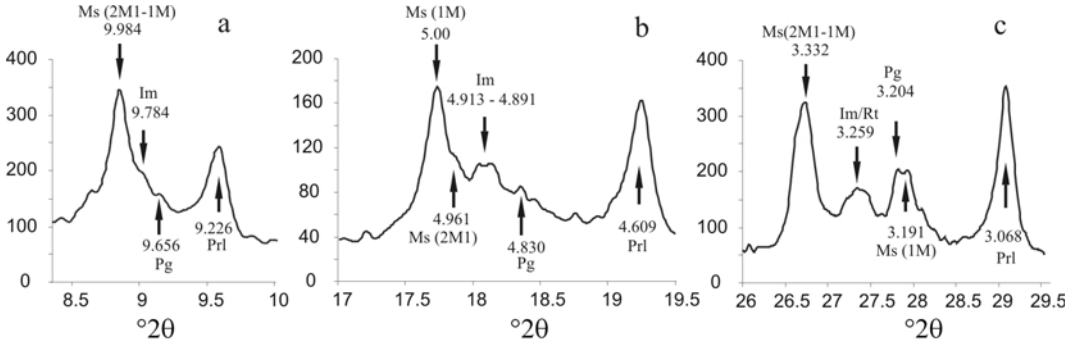

FIG. 5. Selected sections of XRD patterns of basement altered at the TLPU, profile from east of Inca Huasi ranch. Reflection peaks for basal spacing (Å). Abbreviations: muscovite (Ms), intermediate Na-K white mica (Im), paragonite (Pg), pyrophyllite (Prl) and rutile (Rt).

reflection peak for d_{004} of Im ranges over 4.895−4.891 Å and for Pg is 4.83 Å (Fig. 5b). In Fig. 5c a wide peak corresponding to 3.259 Å is assigned to Im and rutile (microscopically identified). The *d* spacing of 3.204 Å is identified as a sixth-order basal reflection of paragonite. These reflection peaks fit well with those of metastable intermediate K-Na white micas (Giorgetti *et al.*, 2003; Jiang & Peacor, 1993).

Geochemistry of REE on alteration profiles

Chemical changes of bulk-rock analyses of progressively altered rocks at the TLPU were described and linked to secondary mineral parageneses (Dristas *et al*, 2003; Dristas & Martínez, 2007; Martínez & Dristas, 2007). In the 8 m thick alteration profile, NE of Inca Huasi ranch (Fig. 1, point 9), a final mass loss of 54% was calculated by applying the isocon method (Martínez & Dristas, 2007) and is thought to result from metasomatism.

Following the behaviour of other chemical elements, trace elements show a common tendency according to type and pervasiveness of alteration. *REE* data are shown in Table 2. The unaltered migmatite from the NE of the Inca Huasi ranch contains 188 ppm Ce. This relatively large value points to monazite and/or allanite, the former being identified by EMPA. The rock displays a prominent negative Eu anomaly (Eu/Eu* = 0.24) (Fig. 6a) with *LREE* enrichment and Σ*REE* ~400 ppm. The fresh basement from the Cerro Gruta de Oro hill and the range of La Siempre Verde ranch also display negative Eu anomalies. These anomalies point to plagioclase with Eu^{3+} fractionated during magmatic crystallization or to a migmatite-melting formation. Thus, bulk-rock analyses would represent residual liquids. On the other hand, incipiently altered samples of basement with chlorite, calcite and sericite as secondary minerals have a steeply positive Eu anomaly (<Eu/Eu* = 11.7), but otherwise an inherited pattern of *REE* (Fig. 6b). Such incipiently altered samples are generally located far from the TLPU. Positive Eu anomalies could be explained by the incorporation of this element in the calcite structure (Stumpf *et al.*, 2007).

The intense basement alteration close to the TLPU results in an enrichment of mainly *LREE* with a positive Ce anomaly clearly apparent in one sample from the Cerro del Medio hill (Ce/Ce*= 5.89) (Fig. 6c). The different behaviour of oxidized cerium (Ce^{4+}) allows fractionation of this element from other *REE* with 3+ valencies (Brookins, 1989). The La/Lu ratios of 17.34 and 6.16 respectively for the samples furthest from and nearest to the TLPU is registered in the Cerro del Medio hill profile.

REE patterns related to a strong phyllic alteration, involving samples of the basement and the base of the sedimentary succession, are shown in Fig. 6d (with Σ*REE* >4600 ppm for the profile of Cerro del Medio). Relatively large *LREE* (La, Ce, Pr, Nd and Eu) concentrations are discernible at the TLPU to the NE of Inca Huasi ranch, where the positive Ce anomaly is gradually enhanced in altered basement approaching the TLPU. This enrichment of *LREE*, seen in several alteration profiles, is due to APS minerals in most altered rocks at the TLPU. On the other hand, heavily

TABLE 2. Bulk-rock chemical analyses of *REE* (in ppm) from fresh basement and altered rocks from the TLPU.

Locality	— Northeast of Inca Huasi —				North of Cerro del Medio Hill				Gruta de Oro
Sample	0524	0824	1024	1324	0122	0322	0322s	0422	0405
La	93.40	6.63	36.30	200.00	4.50	649	356	25.20	92.50
Ce	188.00	10.80	88.10	506.00	62.40	>3000.00	>3000.00	126.00	183.00
Pr	20.80	1.06	9.68	47.40	1.50	143.00	105.00	5.00	18.00
Nd	67.20	3.30	37.90	158	5.00	557.00	466.00	14.80	60.20
Sm	10.10	0.43	6.42	27.10	1.23	136	118	2.40	7.77
Eu	0.64	1.31	1.60	6.00	0.51	46.20	43.40	0.55	1.24
Gd	6.22	0.27	4.82	16.80	1.82	54.00	45.00	1.39	5.28
Tb	0.63	0.03	0.52	1.97	0.35	4.28	5.81	0.20	0.81
Dy	2.60	0.13	2.36	7.58	2.23	12.50	22.80	1.06	3.84
Ho	0.44	0.03	0.42	0.99	0.46	1.33	3.12	0.19	0.72
Er	1.29	0.10	1.15	2.24	1.46	3.46	7.77	0.52	2.38
Tm	n.a	n.a.	n.a	n.a	0.26	b.l	1.12	0.08	0.37
Yb	n.a	n.a.	n.a	n.a	1.77	2.76	7.33	0.51	2.31
Lu	n.a	n.a.	n.a	n.a	0.26	0.27	0.94	0.08	0.33
Σ*REE*	390.03	23.99	215.12	1166.87	83.70	>4610	>3829	177.94	378.75

Locality	North of LSV ranch			Cerro Chico Hill			North of Cuchilla de Aguilas range		
Sample	11211	1319	1119	0503	0403	0218	0604	0704	0804
La	12.80	31.00	38.20	11.70	57.10	8.00	41.00	38.50	161.00
Ce	24.10	181.00	98.40	19.20	183.00	16.20	49.40	57.50	333.00
Pr	10.20	8.18	9.63	1.80	18.90	2.40	7.90	7.70	35.00
Nd	1.80	33.50	36.5	6.00	101.00	10.90	21.00	21.10	116.00
Sm	1.88	7.93	6.97	0.86	28.6	2.96	1.85	2.01	15.20
Eu	1.33	3.06	0.52	1.77	8.27	2.15	0.37	0.44	3.70
Gd	0.15	7.59	4.92	0.50	24.60	3.12	1.56	1.54	9.40
Tb	0.72	0.99	0.68	0.06	3.28	0.47	0.13	0.14	1.11
Dy	0.13	4.17	3.40	0.36	12.60	2.29	0.63	0.69	4.40
Ho	0.33	0.62	0.67	0.09	1.82	0.39	0.11	0.13	0.68
Er	n.a	1.41	1.95	0.31	4.22	0.92	0.32	0.37	1.80
Tm	n.a	b.l	b.l	0.06	0.50	0.12	0.05	0.06	0.25
Yb	n.a	b.l	b.l	0.48	2.72	0.73	0.31	0.38	1.59
Lu	n.a	b.l	b.l	0.10	0.36	0.10	0.05	0.06	0.23
Σ*REE*	56.18	279.45	201.84	43.27	446.97	50.68	124.72	130.56	683.36

b.l. – below detection limit
n.a. – not analysed.

cemented quartz arenites display similar *REE* patterns, but more diluted by their quartz contents (Fig. 6e).

The components of APS minerals identified in backscattered electron images and by EDS analyses (Fig. 3c) range between the end members florencite ($REEAl_3H(PO_4)_2(OH)_6$) and svanbergite ($SrAl_3(PO_4/SO_4)(OH)_6$). The crystal structures of APS minerals are suitable for introducing *REE*, Sr and Ba substitution, since these cations are situated in large cavities formed by 6-membered rings of $M(O,OH)_6$ octahedra (Radoslovich & Slade, 1980).

DISCUSSION

The most outstanding characteristic of the alteration is its zoning, with a widespread overall alteration pattern of newly formed K-white mica + chlorite + calcite ± anatase-rutile ± secondary quartz further from the TLPU, and pyrophyllite + K-white mica + hematite-goethite ± APS minerals ± tourmaline ± anatase-rutile closer to the TLPU. This zoning is asymmetrically developed, probably due to the smaller reactivity of quartz-rich sandstones of the LTF (Frisicale & Dristas, 1993) compared with the basement. The bulk-rock geochemistry of *REE* in

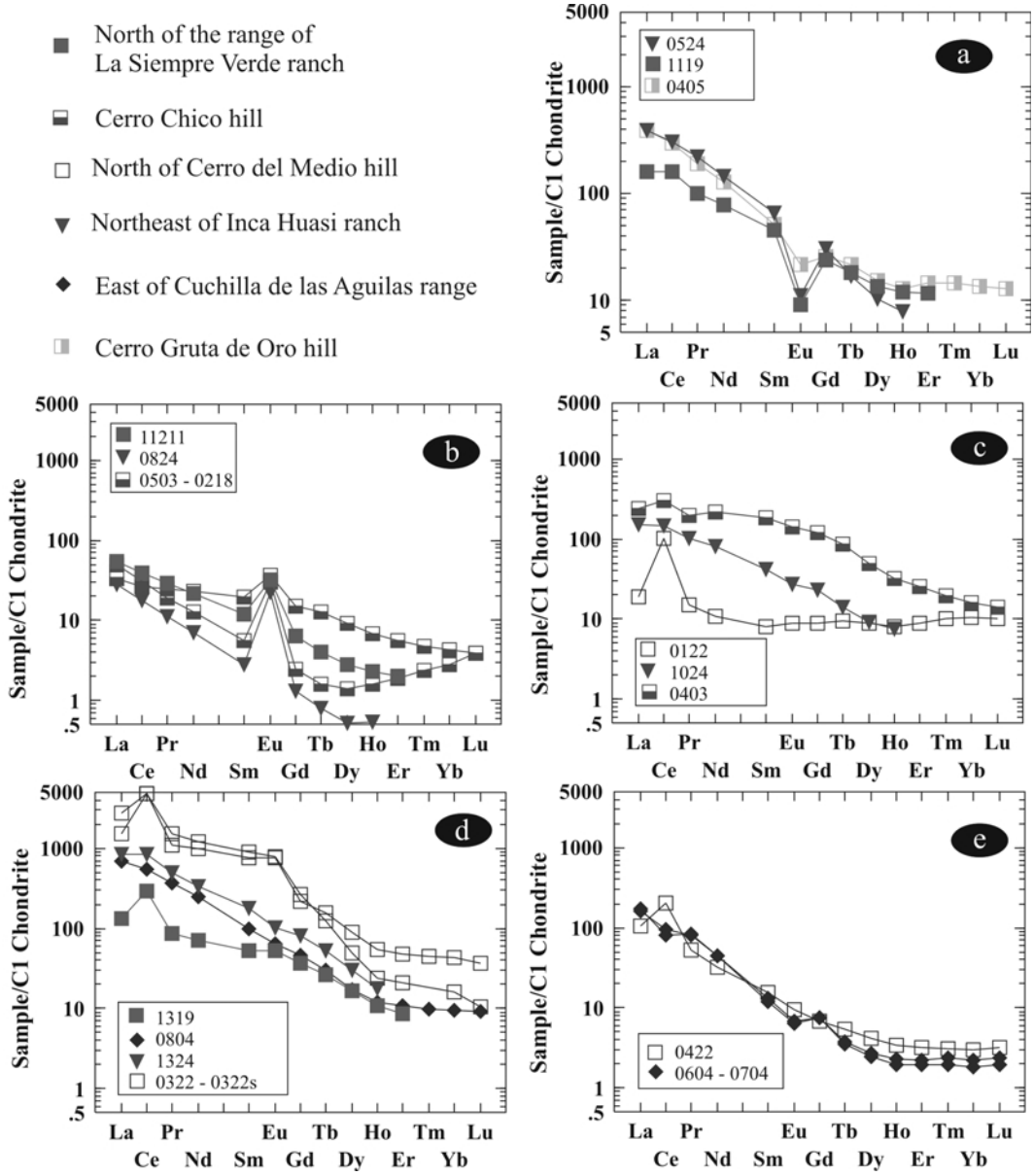

FIG. 6. *REE* distribution patterns normalized to chondrite (C1) for altered basement and sedimentary succession at the TLPU. (a) Fresh basement from NE of Inca Huasi ranch, Cerro Gruta de Oro hill and the range from La Siempre Verde ranch. (b) Incipiently chloritized, carbonatized and sericitized basement furthest from the TLPU. (c) Moderately to intensely altered samples of basement successively close to the TLPU. (d) Greatest intensity of alteration of basement and one sample of intensely altered sandstone at the TLPU. (e) Quartz arenite with scarce clay alteration matrix.

clay mineral assemblages also displays signature changes. An increase in *REE*, especially in *LREE* (La, Ce, Pr, Nd and Eu), towards the TLPU where the intensity of alteration is generally greater is seen. Nevertheless, each alteration profile shows particular characteristics such as the absence or

presence of: (1) silicification; (2) secondary pyrophyllite with or without K-Na contents; (3) K-white micas with more or less limited paragonite contents; (4) discrete quantities of intermediate K-Na white mica; (5) discrete quantities of paragonite; and (6) *LREE*-bearing APS minerals.

For each altered profile, similarities in the chemistry of secondary K-white micas and pyrophyllite on both sides of the unconformity strengthen the idea of hydrothermal fluid circulation through the TLPU, as was previously indicated by common replacement textures (Dristas & Martínez, 2007; Martínez & Dristas, 2007).

Monazite (Fig. 3d) from the unaltered local basement and sedimentary rocks is now identified as one of the main source for *REE*. Mobilization of *REE* on progressively altered rocks at the TLPU is manifested by a very regular behaviour through alteration profiles, except for Ce and Eu. These elements show significant deviations attributable to incorporation Ce and Eu in APS mineral and calcite structures, respectively. The concentrations of *LREE* are directly related to the existence of APS minerals in the clay mineral assemblage. This group of minerals is more stable in lower-pH environments (in which *LREE* are relatively mobile) than apatite (Stoffregen & Alpers, 1987) and result from the interaction of oxidizing and relatively acid fluids with aluminous host rocks enriched in monazite (Gaboreau *et al.*, 2005). Apatite and monazite are the main P sources for APS mineral formation since these minerals are absent where APS minerals are present in the most altered rocks.

The occurrence of APS minerals is closely related to pyrophyllite-bearing mineral parageneses at the TLPU. The temperature of the initial appearance of pyrophyllite will be controlled by pressure and H_2O activity (Frey, 1987). Hence, for an H_2O activity of 0.8, pyrophyllite will appear at ~260ºC at 1 kbar. But for H_2O activity in the order of 0.1−0.2, pyrophyllite is stabilized at the expense of kaolinite + quartz at a temperature of ~200ºC. Mineral parageneses including silicification, carbonatization and chloritization indicate still lower temperatures which seem to be generally attained a few metres away from the TLPU. Homogenization temperatures of fluid inclusions gave temperatures of 90−160ºC in secondary quartz of the silicified basement (Martínez & Dristas, 2007) and 100−150ºC for quartz veins in sandstones at the TLPU (Dristas & Martínez, 2007). This scheme of alteration might have occurred under relatively alkaline conditions and generally further from possible hotter fluid circulation, in zones of lower porosity due to poor hydrothermal lixiviation.

An increase in Na_2O in the most altered rocks of the NE of the Inca Huasi ranch suggested the existences of Na-bearing micas (Martínez & Dristas, 2007). In the present contribution, white micas and pyrophyllite of the hydrothermally altered rocks of the TLPU have been chemically characterized. Backscattered electron images identify Na-bearing potassic white micas and pyrophyllite with Na-K contents as separate phases. XRD spectra of bulk-rock powder samples point to the existence of muscovite ($2M_1$-1M), pyrophyllite, and discrete quantities of intermediate K-Na white mica and paragonite.

Intermediate K-Na white micas could represent metastable phases of the hydrothermal alteration of plagioclase (Jiang & Peacor, 1993; Giorgetti *et al.*, 2003). In such cases, intermediate Na-K white micas result from the incomplete transformation of K-white mica to Na-rich white mica (paragonite). Cation substitutions in pyrophyllite are generally rare (Newman & Brown, 1987), although the existence of pyrophyllite with Na-K contents is well documented in hydrothermal systems. In the active hydrothermal field of PACMANUS, Papua New Guinea, Lackschewitz *et al.* (2004) recognized pyrophyllites with up to 0.30 Na a.p.f.u. with a maximum of ~0.50 a.p.f.u. of alkali and alkaline earth elements. The anomalous large Na-K values in our pyrophyllite chemical analyses (<0.7 a.p.f.u) are not reliable for explaining a solid solution. Therefore, possible nano-lamellar intergrowth with intermediate K-Na mica and/or paragonite on scales below the spatial resolution of the EMP is suggested.

The occurrence of Na-K white micas in low-grade metamorphic rocks, such as in the Central Swiss Alps and Central Wales, seem to be linked to thick sedimentary sequences (Frey, 1987; Li *et al.*, 1994; Livi *et al.*, 1997; Merriman, 2002). On the contrary, the clay mineral assemblages present in the TLPU zone are restricted to zones <20 m wide. Intermediate K-Na white mica, paragonite and pyrophyllite with Na-K contents occur only locally as in the NE of the Inca Huasi ranch. Accordingly, the chemical and mineralogical variations either vertically, a few metres below and above the TLPU, or in different alteration profiles, cannot be related to prograde metamorphism.

The alteration model for these clay mineral assemblages is comparable with that established

for unconformity-type U deposits in the Northern Territory of Australia and the Athabasca Basin of Canada (Komninou & Sverjensky, 1995; Lorilleux *et al.*, 2003; Beaufort *et al.*, 2005; Gaboreau *et al.*, 2005). In the U deposits, the alteration that involves an intense dissolution of earlier silicates (including quartz) and the marked transformation of both sedimentary and metamorphic rocks above and below the unconformity to clay-mineral assemblages, was attributed to large-scale hydrothermal fluid flow. The corresponding hydrothermal fluids circulated at temperatures of 150−300ºC through sandstone aquifers with an unusually high oxidation state (Komninou & Sverjensky, 1995).

CONCLUSIONS

(1) Distribution patterns of clay mineral assemblages, common replacement textures in sandstones and basement rocks, *REE* concentration and chemistry of dioctahedral micas on both sides of the TLPU point to hydrothermal fluid circulation through this unconformity.

(2) According to stability relations for mineral parageneses with APS minerals and pyrophyllite, the hydrothermal fluid can be characterized as acid, oxidized and of relatively high temperature. This fluid acted immediately at the contact. However, mineral parageneses with chlorite, calcite and quartz some metres away from the TLPU formed from fluids neutralized and/or with lower temperature.

(3) This contribution is the first description of the limited occurrence of intermediate K-Na white micas and paragonite in the maximum lixiviation zone at the TLPU. This mineral assemblage supports an environment of hydrothermal activity and suggests crystallization of these minerals under metastable conditions. No conclusions can be drawn on the chemistry of the abnormally large K-Na contents of pyrophyllite and K-white micas with Na until TEM studies have been applied, although nano-lamellar intergrowth with K-Na micas and/or paragonite is suggested.

ACKNOWLEDGMENTS

We are grateful to the Alexander von Humboldt Foundation (3.4 -Fokoop−ARG/1005880), Comisión de Investigaciones Científicas de la provincia de Buenos Aires (CIC), Consejo Nacional de Investigaciones Científicas y Técnicas (CONICET), Agencia Nacional de Promoción Cientifica y Tecnológica (ANPCYT) (PICT 2006/246) and Universidad Nacional del Sur of Argentina (UNS) for providing funds and materials. We are also indebted to the Deutscher Akademischer Austausch Dienst (DAAD) for granting a short-stay fellowship at the Institut für Mineralogie und Kristallchemie, Universität Stuttgart, to J.C.M. The authors acknowledge comments and corrections made by the editors and anonymous referees which helped to improve the manuscript.

REFERENCES

Andreis R.R., Zalba P.E. & Iñiguez-Rodriguez A.M. (1992) Paleosuperficies y sistemas depositacionales en el Proterozoico Superior de la región de Sierras Bayas, Sierras Septentrionales de la provincia de Buenos Aires, Argentina. *Cuarta Reunión Argentina de Sedimentología*, **1**, 283−290.

Beaufort D., Patrier P., Laverret E., Bruneton P. & Mondy J. (2005) Clay alteration associated with Proterozoic unconformity-type uranium deposits in the East Alligator Rivers uranium deposits, Northern Territory, Australia. *Economic Geology*, **100**, 515−536.

Bonhomme M.G. & Cingolani C.A. (1980) Mineralogía y geocronología Rb-Sr y K-Ar de fracciones finas de la 'Formación La Tinta', provincia de Buenos Aires. Asociación Geológica Argentina. *Revista*, **35**, 519−538.

Brookins D.G. (1989) Aqueous geochemistry of rare earth elements. Pp. 201−225 in: *Geochemistry and Mineralogy of Rare Earth Elements* (B.R. Lipin & G.A. McKay, editors), Reviews in Mineralogy and Geochemistry, **21**. Mineralogical Society of America..

Cingolani C.A. & Dalla Salda L. (2000) Buenos Aires cratonic region. Pp. 139−147 in: *Tectonic Evolution of South America* (U.G. Cordani, E.J. Milani, A.T. Filho & D.A. Campos, editors), Rio de Janeiro.

Delpino S.H. & Dristas J.A. (2008) Dolomitic marbles and associated calc-silicates, Tandilia belt, Argentina: Geothermobarometry, metamorphic evolution, and P-T path. *Journal of South American Earth Sciences*, **25**, 501−525.

Di Paola E.C. & Marchese H.G. (1975) Relación entre la tectonosedimentación, litología y mineralogía de arcillas del complejo Buenos Aires y la Formación La Tinta (Prov. de Buenos Aires). *Revista* de *la Asociación Argentina de Mineralogía, Petrología y Sedimentología*, **5**, 3-4, 45−58.

Dristas J.A. & Frisicale M.C. (1984) Estudio de los yacimientos de arcilla del cerro Reconquista, San Manuel, Sierras Septentrionales de la Provincia de Buenos Aires. *9º Congreso Geológico Argentina, S. C. de Bariloche. Actas*, **5**, 507−521.

Dristas J.A. & Frisicale M.C. (1992) Breccias associated with hydrothermal clay deposits, Barker, Tandilia, Bs. As. Argentina. *Zentralblatt für Geologie und Paläontologie Teil I*, **6**, 1901–1915.

Dristas J.A. & Martínez J.C. (2007) Late Proterozoic unconformity-related hydrothermal iron deposits in the north Barker area (Tandilia ranges, Argentina). *Neues Jahrbuch für Geologie und Paläontologie Abhandlungen*, **246**, 267–281.

Dristas J.A., Frisicale M.C. & Martínez J.C. (2003) High REE APS minerals associated with advanced argillic alteration in Cerrito de la Cruz clay deposit, Barker, Buenos Aires province, Argentina. *Göttingen Arbeiten zur Geologie und Paläontologie*, **5**, 1–6.

Fleet M.E. (2003) Sheet silicates: micas. Pp. 41–297 in: *Rock-Forming Minerals*, 2nd ed. (W.A. Deer, R.A. Howie & J. Zussman, editors), Vol. **3A**. The Geological Society, London.

Frey M. (1987) Very low-grade metamorphism of clastic sedimentary rocks. Pp. 9-58 in: *Low-temperature Metamorphism* (M. Frey, editor.), Blackie and Sons, Glasgow.

Frisicale M.C. (1991) *Estudio de algunos yacimientos de arcilla originados por actividad hidrotermal, en las Sierras Septentrionales de la provincia de Buenos Aires.* PhD thesis, Universidad Nacional del Sur, Bahía Blanca, Argentina.

Frisicale M.C. & Dristas J.A. (1993) Alteración hidrotermal en el contacto entre el basamento y la secuencia sedimentaria, en el Cerrito de la Cruz, Tandilia. *12º Congreso Geológico Argentino y II Congreso de Exploración de Hidrocarburos. Actas VII*, **5**, 222–228.

Gaboreau S., Beaufort D., Viellard P. & Patrier P. (2005) Aluminium phosphate sulfate minerals associated with Proterozoic unconformity-type uranium deposits in the East Alligator River uranium field, Northern Territories, Australia. *The Canadian Mineralogist*, **43**, 813–827.

Giorgetti G., Monecke T., Kleeberg R. & Herzig P.M. (2003) Intermediate sodium-potassium mica in hydrothermally altered rocks of the Waterloo deposit, Australia: a combined SEM-EMP-XRD-TEM study. *Contributions to Mineralogy and Petrology*, **146**, 159–173.

Jiang W-T. & Peacor D.R. (1993) Formation and modification of metastable intermediate sodium potassium mica, paragonite, and muscovite in hydrothermally altered metabasites from northern Wales. *American Mineralogist*, **78**, 782–793.

Komninou A. & Sverjensky D.A. (1995) Hydrothermal alteration and chemistry of ore-forming fluids in an unconformity-type uranium deposit. *Geochimica et Cosmochimica Acta*, **59**, 2709–2723.

Lackschewitz K.S., Devy C.W., Stoffers P., Botz R., Eisenhauer A., Kummetz M., Schmidt M. & Singer A. (2004) Mineralogical, geochemical and isotopic characteristic of hydrothermal alteration processes in active, submarine, felsic-hosted PACMANUS field, Manus Basin, Papua New Guinea. *Geochimica et Cosmochimica Acta*, **68**, 4405–4427.

Leveratto M.A. & Marchese H.G. (1983) Geología y estratigrafía de la Formación La Tinta (y homólogas) en el rea clave de Sierra de la Tinta-Barker-Villa Cacique-Arroyo Calaveras, prov. de Buenos Aires. *Asociación Geológica Argentina, Revista*, **38**, 235–247.

Li G., Peacor D.R., Merriman R.J. & Roberts B. (1994) The diagenetic to low-grade metamorphic evolution of matrix white mica in the system muscovite-paragonite in a mud-rock from Central Wales, United Kingdom. *Clays and Clay Minerals*, **42**, 369–381.

Livi K.J.T., Veblen D.R., Ferry J.M. & Frey M. (1997) Evolution of 2:1 layered silicates in low-grade metamorphosed Liassic shales of central Switzerland. *Journal of Metamorphic Geology*, **15**, 323-344.

Lorilleux G., Cuney M., Jébrak M., Rippert J.C. & Portella P. (2003) Chemical brecciation processes in the Sue unconformity-type uranium deposits, Eastern Athabasca Basin (Canada). *Journal of Geochemical Exploration*, **80**, 241–258.

Manassero J.M. (1986) Estratigrafía y estructura en el sector oriental de la localidad de Barker, Provincia de Buenos Aires. *Asociación Geológica Argentina, Revista*, **41**, 375–385.

Martínez J.C. & Dristas J.A. (2007) Paleoactividad hidrotermal en la discordancia entre el Complejo Buenos Aires y la Formación La Tinta en el rea de Barker, Tandilia. *Asociación Geológica Argentina, Revista*, **62**, 375–386.

Massonne H.-J. (1995) III. Rhenohercynian Foldbelt, C. Metamorphic units (northern phyllite zone), 4. Metamorphic evolution. Pp. 132–137 in: *Pre-Permian Geology of Central and Eastern Europe* (R.D. Dallmeyer, W. Franke & K. Weber, editors). Springer, Berlin.

Merriman R.J. (2002) Contrasting clay mineral assemblages in British Lower Palaeozoic slate belts: the influence of geotectonic setting. *Clay Minerals*, **37**, 207–219.

Newman A.C.D. & Brown G. (1987) The chemical constitution of clays. Pp. 1–48 in: *Chemistry of Clays and Clay Minerals* (A.C.D. Newman, editor). Monograph **6**, Mineralogical Society, London.

Pankhurst R.J., Ramos V.A. & Linares E. (2003) Antiquity of the Río de la Plata Craton in Tandilia, southern Buenos Aires province, Argentina. *Journal of South American Earth Sciences*, **16**, 5–13.

Radoslovich E.W. & Slade P.G. (1980) Pseudotrigonal symmetry and the structure of gorceixite. *Neues Jahrbuch für Mineralogie, Monatshefte*, 157–160.

Reed S.J.B. & Buckley A. (1998) Rare earth element

determination in minerals by electron-probe microanalysis: application of spectrum synthesis. *Mineralogical Magazine*, **62**, 1–8.

Rieder M., Cavazzini G., D'Yakonov Y.S., Frank-Kamenetskii V.A., Gottardi G., Guggenheim S., Koval P.V., Müller G., Neiva A.M.R., Radoslovich E.W., Robert J-L., Sassi F.P., Takeda H., Weiss Z. & Wones D.R. (1998) Nomenclature of the micas. *Clays and Clay Minerals*, **46**, 586–595.

Shau Y-H., Feather M.E., Essene E.J. & Peacor D.R. (1991) Genesis and solvus relations of submicroscopically intergrown paragonite and phengite in blueschist from northern California. *Contributions to Mineralogy and Petrology*, **106**, 367–378.

Stoffregen R.E. & Alpers C.N. (1987) Woodhouseite and svanbergite in hydrothermal ore deposits: product of apatite destruction during advanced argillic alteration. *The Canadian Mineralogist*, **25**, 201–211.

Stumpf T., Marques Fernandes M., Walther C., Schmidt M., Dardenne K., Bosbach D. & Fanghänel T. (2007) Structural incorporation of Eu(III) into calcite: process understanding on a molecular level. 7th Annual V. M. Goldschmidt Conference, Köln. *Geochimica et Cosmochimica Acta*, **71**, Suppl. S, A160.

Zalba P.E. & Andreis R.R. (1998) Basamento saprolitizado y secuencia sedimentaria suprayacente en San Manuel, Sierras Septentrionales de Buenos Aires, Argentina. *VII Reunión Argentina de Sedimentología*, Salta, *Actas*, 143–154.

Zalba P.E., Andreis R.R. & Lorenzo F.C. (1982) Consideraciones estratigraficas y paleoambientales de la secuencia basal Eopaleozoica de la Cuchilla de Las Aguilas, Barker, Argentina. *V Congreso Latinoamericano de Geología, Argentina*, **2**, 389–409.

Zalba P.E., Poiré D.G., Andreis R.R. & Iñiguez-Rodríguez A.M. (1992) Precambrian and Lower Paleozoic records and paleosurfaces of the Tandilia system, Buenos Aires province, Argentina. Mineralogical and geochemical records of paleoweathering. *Mémoire des Sciences de la Terre*, **18**, 153–161.